JOURNAL OF GEOPHYSICAL RESEARCH, VOL. 101, NO. D7, PAGES 12,667–12,683, MAY 20, 1996

Use of on-line tracers as a diagnostic tool in general circulation model development
1. Horizontal and vertical transport in the troposphere

David Rind and Jean Lerner[1]
NASA Goddard Space Flight Center, Institute for Space Studies, New York

Abstract. The use of passive on-line tracers in a general circulation model (GCM) developmental process is discussed. CFC-11 and ^{85}Kr are used to evaluate interhemispheric transport. It is shown that new boundary layer and convective parameterizations lead to reductions in the interhemispheric exchange times to values in close agreement with observations of little more than one year. Radon 222 is used to evaluate vertical mixing away from the surface. The new convection scheme produces smaller convective fluxes, which substantially reduce the high-altitude concentrations of ^{222}Rn equatorward of 30° latitude. While this result is in better agreement with other models, scarcity of observations prevent any conclusion as to which formulation is more accurate. The effect of altered numerical schemes for solution of the momentum and energy equations in the GCM is shown to have little influence on the model's interhemispheric transport or vertical mixing. Finer vertical resolution increases convective mixing of ^{222}Rn somewhat and allows for larger pollution concentrations of CFC-11 in the boundary layer. Employing on-line passive tracers in the course of model development should allow for improvements in a GCM's horizontal and vertical fluxes and optimization of the model for atmospheric chemistry purposes.

1. Introduction

The continued development of general circulation models (GCMs) is done with two goals in mind: increasing the realism of the modeled processes and improving the accuracy of the simulated current climate and its variability. The latter is accomplished by a continual comparison of model results with observations. Invariably, the model result which is most closely perused is that which is thought important for the subsequent model use; for example, when climate change experiments are the intended object, parameters most important from the climate standpoint receive the greatest attention. In most cases these represent the first-order variables, such as the temperature, precipitation, and cloud cover in specific regions. The model's fluxes are second-order parameters which are compared with observations primarily to understand problems which arise in the target variables.

However, GCMs are now being utilized more frequently for additional studies, in which the fluxes themselves are of prime importance. Three-dimensional chemical tracer models (CTMs) incorporate GCM winds and convective fluxes (and often other parameters, such as radiation fields, temperature, water vapor, and clouds) off-line to advect constituents in both the troposphere and the stratosphere (e.g., studies using the Goddard Institute for Space Studies (GISS) GCM output in CTMs include *Prather et al.* [1987], *Jacob et al.* [1989], *Jacob and Prather* [1990], *Balkanski et al.* [1990, 1992], and *Hall and Prather*, 1993]). Comparisons are made of these tracers with available observations, and conclusions are ultimately drawn concerning the realism of the model transports, potential sources, and sinks [e.g., *Pinto et al.*, 1983; *Fung et al.*, 1983, 1991; *Hartley et al.*, 1994] and deduced photochemical properties of the atmosphere [e.g., *Chin et al.*, 1994].

In many cases the GCM transports are found wanting. In various studies done with transports from the GISS GCM [*Hansen et al.*, 1983] a prime difficulty emerged: the interhemispheric transport was too small, as evaluated by comparing model and observed CFC-11 and CFC-12 concentrations [*Prather et al.*, 1987]. Those authors considered one likely possibility for this deficiency to be intergrid horizontal mixing associated with convection. To improve the performance of the off-line CTM, *Prather et al.* [1987] introduced a diffusion coefficient associated with convective events. This diffusion was not actually in the GCM; had it been so, it would have further altered winds and temperatures. Therefore the added diffusion was inconsistent with the GCM itself. The compensation for the CTM was necessitated by the "after-the-fact" analysis which utilized winds from an already developed GCM.

To avoid this situation, we decided to make tracer transport an integral component of model development evaluation. This involves utilizing on-line tracers and running experiments in conjunction with significant changes in model physics or numerics. The resultant model is therefore a known quantity for tropospheric chemistry purposes, at least for the diagnostics perused. In addition, as we will show, the tracers provide significant information which augments the standard observations used for comparison and are therefore of distinct benefit for model development itself.

In this paper we concentrate on the use of passive tracers to test model horizontal and vertical transports. For modeling horizontal transport we use CFC-11 and ^{85}Kr, both of which have primarily northern hemisphere sources. Vertical trans-

[1]Science Systems and Applications, Inc., New York.

Paper number 96JD00551.
0148-0227/96/96JD-00551$09.00

Table 1. CFC-11 Sources and Sinks in Experiments

	Description
Period of simulation	1986–1991
Initial conditions	zonally uniform mixing ratios (v/v) for April 1, 1986; troposphere (surface to 100 mbar): NH, uniform (20°N–90°N) and 235 ppt; SH, uniform (20°S–90°S) and 220 ppt; tropics, linear with altitude, from 235 ppt (20°N) to 220 ppt (20°S)
Source	total annual flux of 310×10^9 g/yr
Sink	total global sink 90×10^9 g/yr, applied in upper layer only, proportional to the ratio of mass of CFC-11 in the grid box to CFC-11 in the layer as a whole

Spatial Distribution of Source*

Location	Latitude	Longitude	Proportion, %
United States and Canada	30°N–50°N	70°W–125°W	37
Europe and Russia	35°N–65°N	10°W–45°E	37
Far East	20°N–45°N	120°E–150°E	13
Middle East	15°N–35°N	30°E–75°E	5
South America	23°S	45°W	4
South Africa	34°S	20°E	2
Australia and New Zealand	34°S	150°E	2

*Source is emitted uniformly throughout the year. In source regions of NH, emissions are distributed proportional to the land surface area within specified latitude-longitude regions. In the SH, emissions are single grid-box sources. Emissions are put in the lowest model layer (or the surface).

port away from the surface is tested using ^{222}Rn, which has primarily a land source. In section 2 we describe the overall approach. In the following section we indicate the significant model development features which were tested. In section 4 we show how changes in the model affected the tracer distributions. In section 5 we summarize the results.

2. Utilization of on-Line Tracers

The GISS GCM has the capability of providing for sources, sinks, and transport of any number of on-line tracers. For example, tracer transport of on-line water vapor isotopes has been used in numerous studies [*Jouzel et al.*, 1987, 1991; *Cole et al.*, 1993; *Charles et al.*, 1994] to evaluate relevant model processes and comment on paleoclimate reconstructions.

Sources and sinks can be specified as desired, including dependence on GCM conditions. The tracers are advected each dynamic time step by the model winds, generally using the linear upstream scheme [*Russell and Lerner*, 1981]. (A separate test with tracer advection using the quadratic upstream scheme, which is mathematically identical to the second-order moments scheme of *Prather* [1986], is included for comparison). Tracers are also mixed vertically each hour by moist and dry convection. The tracers employed in this paper are passive; that is, their output does not influence the subsequent model simulation and they do not interact with each other.

The tracers were chosen to investigate specific model and chemical transport concerns. CFC-11 and ^{85}Kr were employed to study horizontal, particularly interhemispheric, transport. Radon 222 was used for assessing vertical transport. Following a specification of initial conditions, most experiments were run for 6 model years; results reported here will be for the last 5 years, although in general, the characteristics of the model simulation were evident by the end of the second year. For the features of interest here, a 1-year spin-up is sufficient, as will be shown in the subsequent results.

Incorporation of three on-line tracers increases by 75% the number of independent variables being calculated in the dynamical subroutine; on an IBM RISC workstation, this lengthens the computer time for model integration by approximately 25% at 4° × 5° horizontal resolution. A relevant question is: what is the advantage in using the tracers on-line instead of periodically saving the fluxes off-line for a CTM that could make numerous experiments at a fraction of the computing time? The two options are not mutually exclusive; on-line simulations can help solve many problems associated with off-line applications through direct comparisons. For example, there is the ever-present uncertainty of how frequently the fluxes, particularly convection, need to be saved in order to produce an accurate simulation of the GCM 1-hour time steps, an answer which probably depends on the problem being considered. With many parameters to be saved at each time step, space considerations become a problem, especially if interannual model variability is needed. From the practical standpoint, when the physics of the GCM is changed, it often affects the way the tracer transports must be utilized in the off-line model and perhaps the frequency with which output must be saved. This is especially true of the model's convective parameterization. With the on-line procedure the movement of the tracers is identical to how other quantities (such as heat and moisture) are being transported. To continually modify the off-line model becomes a very time-consuming process; as the convective algorithm becomes more sophisticated/complicated, it becomes increasingly difficult (if not impossible) to parameterize it accurately for off-line use. Presumably, once a final version of the model is agreed upon, modification and utilization of the off-line model, at least for noninteractive tracers, becomes a practical venture.

In addition, there comes a point when the tracers under consideration (such as the water vapor isotopes) become so dependent on GCM processes and variables that on-line incorporation becomes a necessity. Interactive tracers, such as photochemically active species which alter the model's radiative fluxes and dynamic responses, must be an integral part of the GCM.

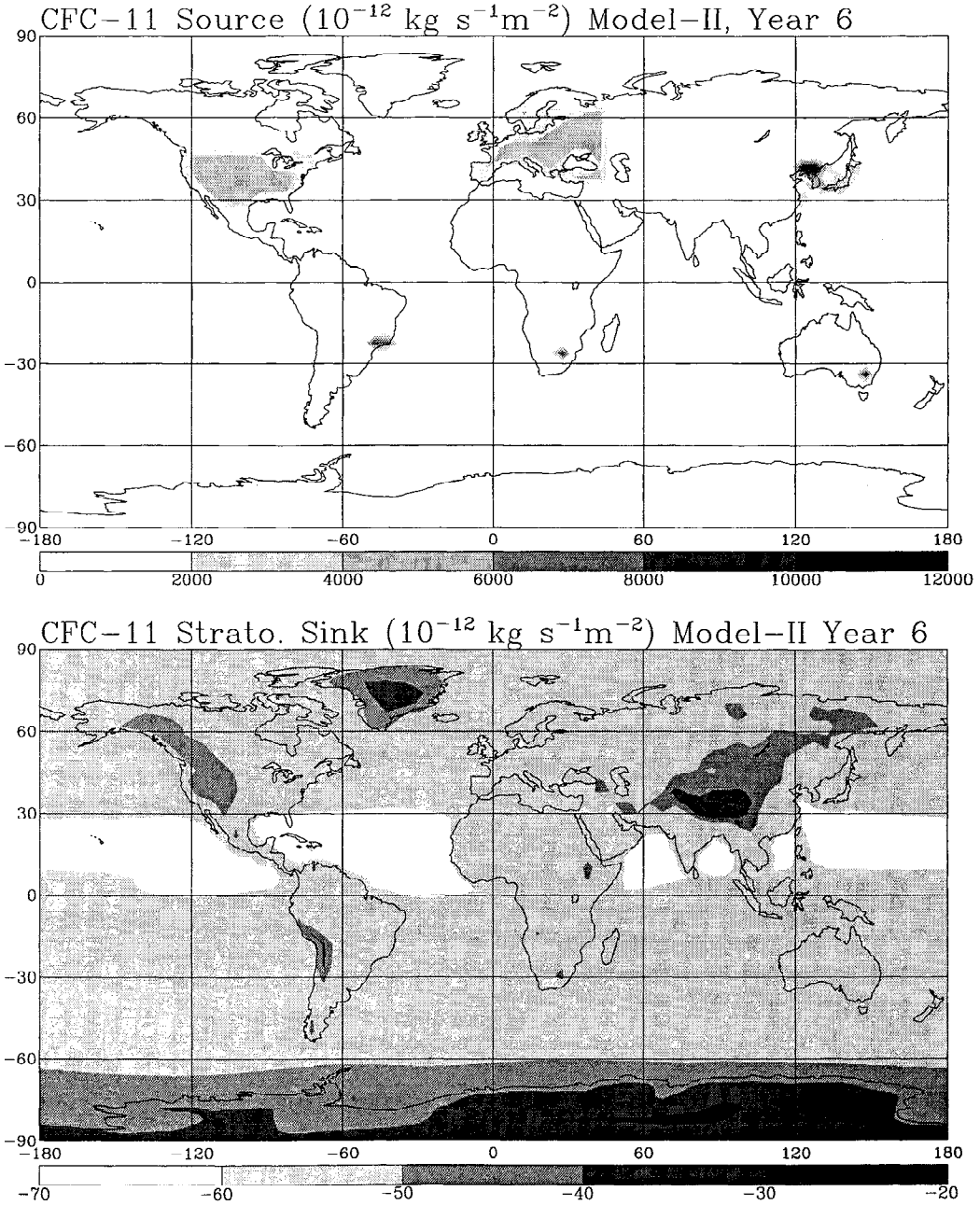

Figure 1. Geographical distribution of annual CFC-11 sources (top) and sinks (bottom).

3. GCM Development

Model development at GISS has been preceding for several years, with the piecemeal implementation of different physics subroutines and numerical schemes. After each substantial change, the on-line tracer code was activated, and the impact of the change on model transports was evaluated. In this paper we will discuss a subset of the experiments, concentrating on the effect of changes in the following modeled processes/numerics: boundary layer, convection, land surface, cloud generation, vertical resolution, heat and moisture advection, and momentum advection. A brief description of the different model schemes follows, as well as an assessment of how the physical/numerical process should be of direct concern for tracer transport. In section 4 we show that indirect influences sometimes have even greater impact than the expected effects.

In the following discussion the term "model II" refers to the *Hansen et al.* [1983] model code run at 4° × 5° resolution; "model II′ physics" refers to this model except that it includes the new convection, boundary layer and land surface parameterizations described below. A version of the model with these plus additional changes was used in the GISS 1994 Summer Institute and is henceforth referred to as the Summer Institute Model (SIM).

3.1. Model II′ Physics

Boundary layer. Model II's dependence on the Ekman length was inaccurate near the equator, since the assumption of an infinite depth modified-Ekman layer was impossible to satisfy when the Coriolis force goes to zero. In addition, the model used crude bulk formulae for surface fluxes and ex-

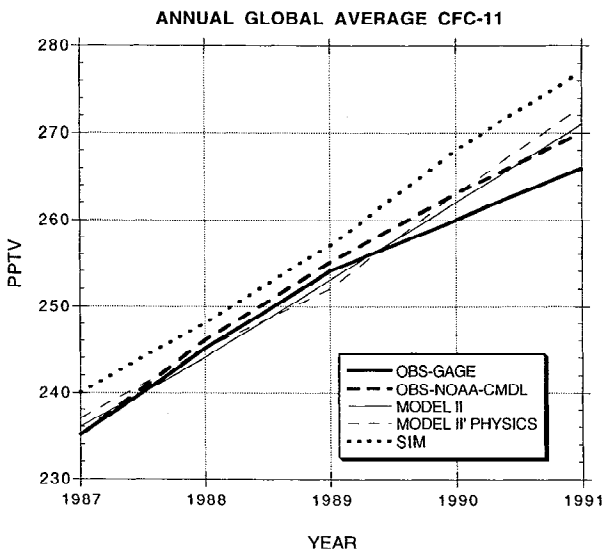

Figure 2. Global, annual average surface CFC-11 concentration as a function of year. Observations are as summarized by *Kaye et al.* [1994].

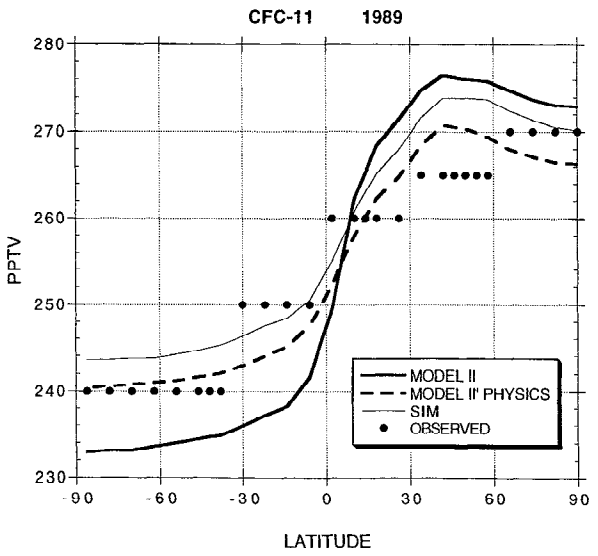

Figure 3. Latitudinal distribution of CFC-11 in lowest model layer for year 6. Observations are from *Kaye et al.* [1994].

change coefficients within the boundary layer. The new boundary layer parameterization employs a finite modified Ekman layer with parameterizations for drag and mixing coefficients based on similarity theory. A complete description of the new boundary layer can be found in the work of *Hartke and Rind* (in preparation, 1995). The primary direct impact on tracer transport of this physics concerns vertical mixing of surface fluxes.

Convection. The convection used in model II raised one-half the mass of the grid box whenever the moist static energy profile became unstable. The new scheme includes variable vertical mass flux made proportional to the instability, one entraining and one nonentraining plume, and explicit downdrafts with mass equal to one-third the updraft [*Del Genio and Yao*, 1992]. The primary impact on tracer transport concerns the vertical mixing associated with convection. An additional question concerns the use of momentum mixing by convection, which alters both the mean circulation and the tropical eddy energy; results are shown both with and without this feature.

Land surface. A new land surface parameterization was added, based on the work of *Abramopolous et al.* [1988] and refined by *Rosenzweig and Abramopolous* [1995]. In contrast to the simplified land surface used in model II the processes of transpiration, evaporation from intercepted precipitation and dew, infiltration, soil water flow, and runoff are explicitly calculated. The primary impact on tracer transport arises indirectly, through the land surface influence on hydrological properties, hence latent heat release, diabatic circulation, and convection.

3.2. Summer Institute Model

In addition to these three fundamental physical changes, various other processes have also come under scrutiny in the course of model development. This includes the incorporation of a cloud liquid water budget and the use of new schemes for the advection of heat, water vapor, and momentum. A version of the model with increased vertical resolution version was also tested.

Large-scale clouds. A cloud liquid-water (CLW) budget scheme was incorporated, with liquid water and ice carried as a prognostic variable [*Del Genio and Yao*, 1995]. Microphysical sources and sinks of cloud water are represented, and an interactive optical thickness calculation is included. The primary direct impact on the tracers discussed here is on atmospheric dynamics associated with cloud radiative forcing.

Heat and moisture advection. The heat and moisture advection, which in model II was accomplished with a second-order-centered differencing scheme, was replaced with a quadratic upstream scheme (QUS), which is mathematically equivalent to the second-order moments scheme of *Prather* [1986] for tracers which can be positive or negative. For tracers which must be positive, the QUS minimizes the adjustments necessary to prevent negative values of fluxes and is therefore less diffusive. As this scheme can preserve strong gradients and hence alter eddy available potential energy and moisture/radiative forcing, its most direct impact on tracer transport is associated with the resulting dynamical response to such variations. In one experiment, the QUS was used for the advection of the tracers, which otherwise were advected using the linear upstream scheme of *Russell and Lerner* [1981].

Momentum advection. For advection in the momentum equation the second-order B grid scheme of *Arakawa* [1972] was replaced by a fourth-order B grid scheme developed by F. Abramopolous (personal communication, 1994). Fourth-order schemes tend to move waves faster [*Kalnay-Rivas et al.*, 1977], so the direct impact should be on intrahemispheric transport and high-frequency synoptic-scale variations.

Vertical resolution. Many processes may be affected by the model's vertical resolution, including the ability to resolve waves with short vertical wavelengths, tropospheric/stratospheric exchange, and boundary layer processes. The standard model has nine vertical layers, as described by *Hansen et al.* [1983]. An 18-layer version of the SIM was run, with the vertical resolution increased substantially near the tropopause (from 3–5 to 1.5 km), in the boundary layer (from 500 to 250m), and in the stratosphere. This version also includes the mountain wave drag parameterization presented by *Rind et al.* [1988]. As these runs were more time consuming, they were generally of shorter duration. The primary impact for the tracers discussed here concerns the ability of higher vertical reso-

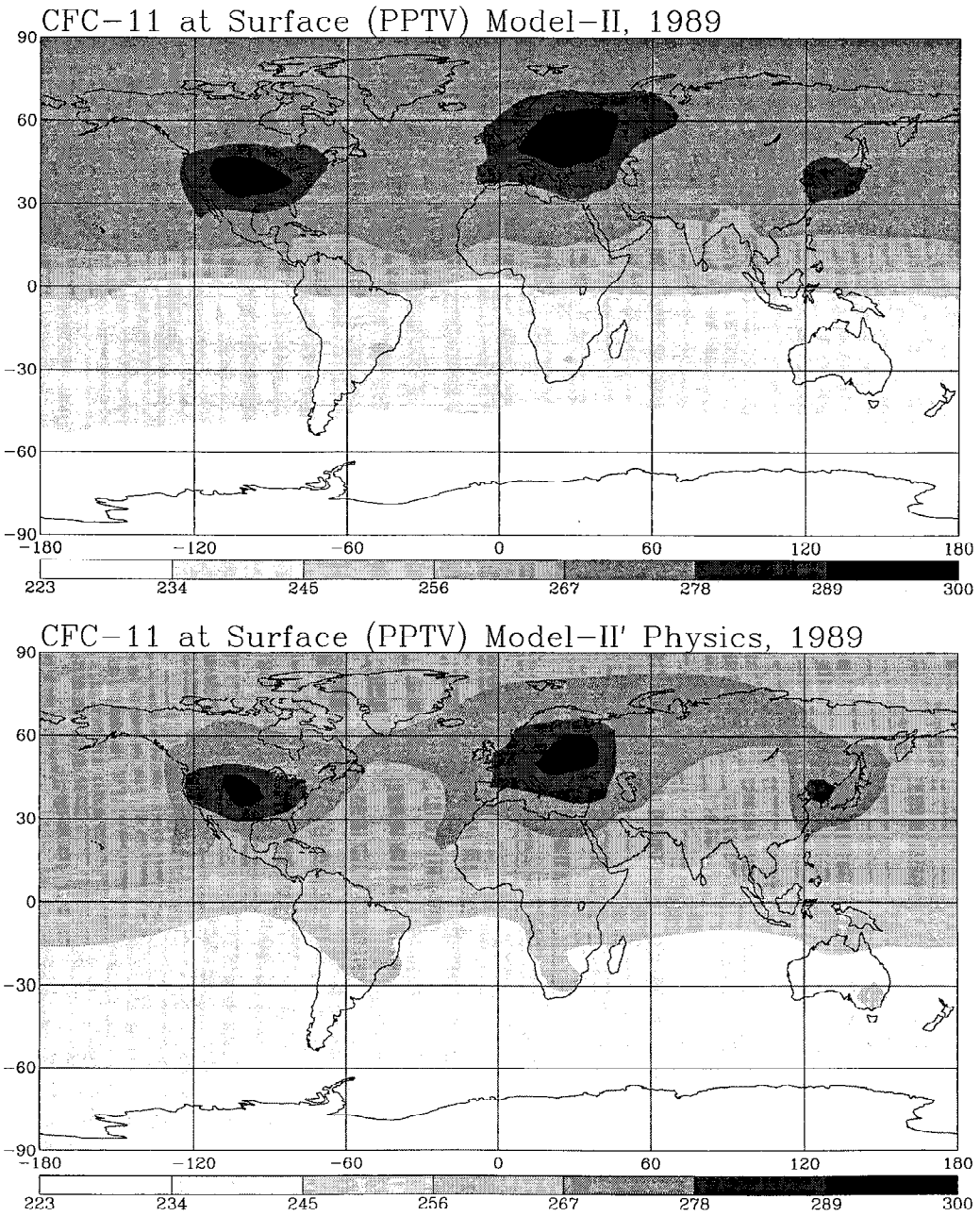

Figure 4. Geographical distribution of CFC-11 for the sixth year in model II (top) and model II′ physics (bottom).

lution to affect atmospheric energetics plus convection and associated horizontal and vertical transports.

4. Tracer Transport Results

4.1. Horizontal Transport

Both CFC-11 and ^{85}Kr have primarily northern hemisphere sources and long tropospheric residence times, which make them good tests of interhemispheric transports.

We begin with CFC-11. A complete description of the period of simulation, initial conditions, source, and sink for this constituent is given in Table 1. These follow the prescriptions given for emissions designed for the WCRP model intercomparison [*Prather*, 1992; *Prather and Remsberg*, 1993]. The geographical distribution of the CFC-11 sources and sinks are shown in Figure 1. The northern hemisphere industrial countries dominate the source; note that emissions are not weighted by population density in the United States and western Europe and hence may not be particularly well suited to address pollution events [*Williamson et al.*, 1992]. The stratospheric sink is greatest in the tropics; the loss of tropospheric constituents to the stratosphere in the tropical region is consistent with observations of CO_2 [*Hall and Prather*, 1993]. As the loss in the upper layer is proportional to the mass of CFC-11 in the grid box, areas of high topography, with smaller mass in the highest layer, have reduced losses.

In Figure 2 the global average concentrations at the surface are shown as a function of time compared with observations from the Global Atmospheric Gases Experiment (GAGE) [*Prinn et al.*, 1983; *Cunnold et al.*, 1983, 1986, 1994; *Kaye et al.*,

Table 2. Krypton 85 Sources and Sinks in Experiments

	Description											
Period of simulation	1978–1983											
Initial conditions												
up to 150 mbar												
latitude	89°N	84°N	76°N	68°N	60°N	52°N	44°N	36°N	28°N	20°N	12°N	4°N
mixing ratio	37	38	38	38	37	37	37	36	35	35	35	35
latitude	89°S	84°S	76°S	68°S	60°S	52°S	44°S	36°S	28°S	20°S	12°S	4°S
mixing ratio	31	31	31	31	32	32	32	32	33	33	33	34
150–70 and 70–10 mbar	values scaled by 0.95 and 0.89, respectively; then all mixing ratios rescaled to obtain a zonal mean mixing ratio $M = 166.2 + 5.10 \times (Y - 1980.0)$ kg, where Y is the initialization time (in units of years A.D.) and 1980.0 is January 1, 1980											
Source	krypton 85 is emitted during reprocessing of nuclear fuel; there were seven known point sources in 1978–1983											
Sink	radioactive decay, with a first-order loss rate constant; $k = 2.0 \times 10^{-9}$ s^{-1} (corresponding to a lifetime of 15.5 years)											

			Annual Mean Emissions, kg/yr					
Source Location	Lat	Long	1978	1979	1980	1981	1982	1983
Savannah, United States	33°N	81°W	1.22	1.17	1.20	1.38	1.43	1.76
Idaho City, United States	44°N	116°W	0.26	0.00	0.23	0.15	0.03	0.00
Sellafield, U.K.	53°N	3°W	1.79	2.40	2.14	3.57	3.03	2.88
Marcoule, France	44°N	4°E	0.79	0.71	1.38	0.79	0.79	0.79
LaHague, France	50°N	2°W	2.01	1.63	2.12	2.32	3.24	4.97
Karlsruhe, Germany	49°N	8°E	0.00	0.13	0.08	0.00	0.00	0.21
TokaiMura, Japan	35°N	140°E	0.15	0.00	0.71	0.28	0.48	0.23
Kyshtym, former USSR	55°N	60°E	9.07	9.61	8.13	7.83	7.65	6.12

1994] and at NOAA CMDL measuring stations (as summarized by *Kaye et al.*, 1994). All the model simulations (including runs not shown here) approximately simulate the change with time, as the specified stratospheric loss rate in combination with the specific sources produced an appropriate net change with time. Note that this is therefore not a test of the stratospheric chemistry, but it does show that the transport into the stratosphere is not grossly inaccurate.

There are specific differences between the models and the observations, however. The annual emissions of 310×10^9 g/yr is representative of 1986 conditions; however, by 1992 the emissions had dropped to about 230×10^9 g/yr [*International Panel on Climate Control (IPCC)*, 1994], in association with enactment of the Montreal Protocol. Since this change was not included in the experiments, none of the model runs showed the declining rates of growth evident in the observations after 1989.

In addition, SIM had consistently higher values by a few parts per trillion by volume (pptv) than the other simulations. This was true not only of the surface values, shown in Figure 2, but also up to 200 mbar. However, the total atmospheric CFC-11 values were practically identical because SIM had reduced transport into the top model layer (though 70 mbar) and hence reduced stratospheric concentrations. The difference arises because of reduced vertical mass transport into the tropical stratosphere in SIM, which occurred when the cloud

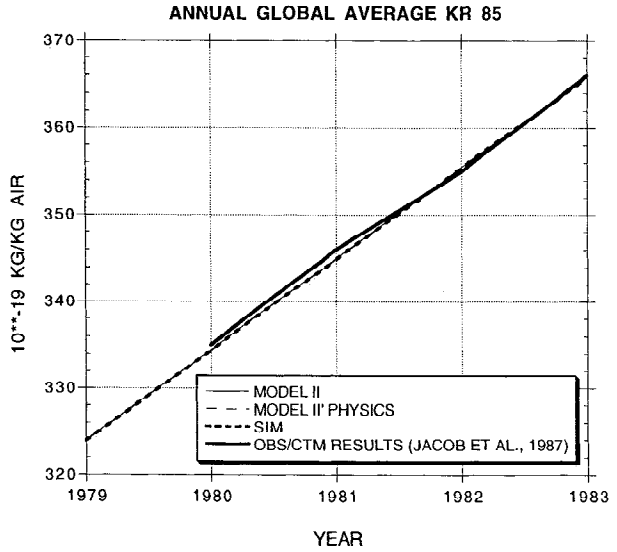

Figure 5. Global, annual average concentration of ^{85}Kr as a function of year.

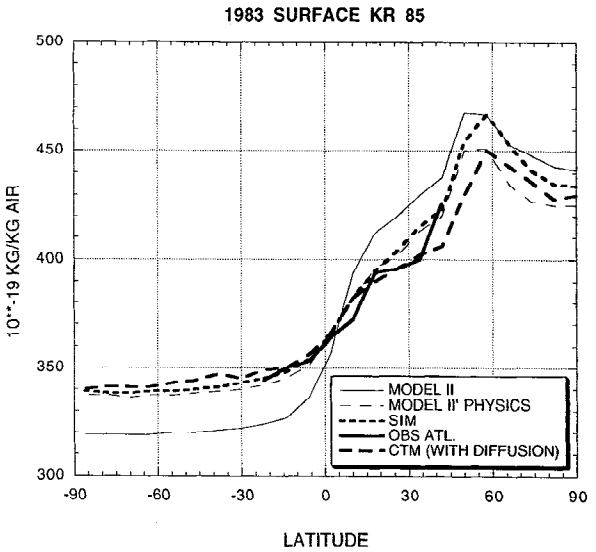

Figure 6. Latitudinal average distribution of ^{85}Kr over the Atlantic Ocean for the sixth year.

Table 3. Interhemispheric Exchange Times for CFC-11 and ^{85}Kr

Year	Model II	II′ Phys	II′ Phys + QUS	II′ Phys + QUS + Mom Mix	SIM	SIM + QUS for Tracer Adv	SIM, 18L
				CFC-11			
2	2.38	1.31	1.35	1.64	1.40	1.46	1.47
3	2.56	1.32	1.27	1.51	1.33	1.45	1.40
4	2.60	1.40	1.31	1.58	1.34	1.36	1.45
5	1.90	1.24	1.30	1.53	1.35	1.49	
6	2.62	1.31	1.30	1.51	1.37	1.48	
Avg	**2.41**	**1.31**	**1.30**	**1.55**	**1.36**	**1.44**	**1.44**
				Krypton 85			
2	2.35	1.31	1.24	1.50	1.31	1.29	1.46
3	2.46	1.32	1.20	1.44	1.26	1.31	1.42
4	2.48	1.36	1.25	1.48	1.27	1.26	1.42
5	2.09	1.27	1.22	1.40	1.25	1.31	
6	2.49	1.30	1.18	1.44	1.28	1.30	
Avg	**2.38**	**1.31**	**1.21**	**1.45**	**1.27**	**1.29**	**1.43**

$t_{exchange} = \Delta C/\phi$(N-S), where ΔC = (NH − SH) concentrations and ϕ(N-S) is net cross-equatorial flux. QUS, quadratic upstream scheme; SIM, Summer Institute model; CTM, chemical tracer model. For CFC-11: CTM, D = 0, ···, 2.60; D = 160–250 km, $\pm_{exchange}$ = 1.10–0.70 (acceptable range) [*Prather et al.*, 1987]. For ^{85}K: CTM, D:180 km, ···, $\pm_{exchange}$ = 1.10 (best) [*Jacob et al.*, 1987].

liquid water budget was added to the model. This new scheme and its interaction with convection altered latent heat release and radiation absorption, with the effect that the tropical mean circulation cells had altered latitudinal distributions at high altitudes. The vertical resolution used in most of these experiments is not sufficient to comment on tropospheric-stratospheric exchange in any detail; we simply note that transports through the tropical tropopause are apparently sensitive to such details in the model.

The latitudinal distribution in the lowest model layer for year 1989 is presented in Figure 3. It can be seen that model II′ physics produced a weaker north-south gradient than model II; the gradient in SIM was similar to that for model II′ physics, although offset by a few pptv. The same differences hold when tropospheric average quantities are considered.

Also shown are the observations, given for latitude bands as in the work of *Kaye et al.* [1994]. The observed values are not latitudinal averages but the result of averaging individual observing stations. Nevertheless, they do indicate the reduced gradient more characteristic of the newer GCM runs.

The geographical distribution for the sixth year for model II (top) and model II′ physics is shown in Figure 4. The cross-equatorial gradient is reduced at all longitudes with model II′ physics.

Table 2 presents the relevant parameters for the ^{85}Kr study. The source is at a few locations in the northern hemisphere, and radioactive decay is the primary sink. The global average change with time for several different model simulations is shown in Figure 5, compared with the CTM analysis of *Jacob et al.* [1987], who obtained estimates of global averages by utilizing observations at selected locations together with model results. The global average change with time is not dependent on model parameterizations due to the simplicity of the sources and sinks, and because the sink is not associated with transport into the stratosphere, SIM produces similar results to the other model experiments.

The latitudinal distribution over the Atlantic Ocean for 1983 is shown in Figure 6, compared with observations. Again the model II′ physics has produced a smaller interhemispheric gradient indicating increased transports, now in good agreement with observations. Note that this result was achieved in the CTM study of *Jacob et al.* [1987] by using model II winds plus specified diffusion associated with convection. Apparently, this diffusion is not needed with the new physics.

A summary of the interhemispheric exchange times is presented in Table 3 for each of the five years of different model development runs, ignoring the spin-up year. (For this discussion we are using the simplification of defining the interhemispheric exchange as that delineated by the equator, rather than by the Intertropical Convergence Zone, whose latitude varies with longitude; this is consistent with the exchange time defined from observations, to which comparison is made.) For both CFC-11 and ^{85}Kr, model II values were 2 times too large, while the new model runs are all close to (although slightly larger than) the "acceptable range," which is derived from observations as discussed by *Prather et al.* [1987] and *Jacob et al.* [1987]. The CTM results shown in the table refer to the off-line experiments incorporating an intergrid diffusion length scale (D) associated with convection. Note that GCM results have stabilized by year 2, as its values are no different from those of subsequent years.

The improvement occurs with the introduction of model II′ physics. Figure 7 (top) shows the ^{85}Kr mean circulation transports as a function of latitude for both model II and model II′ physics in model year 1983. Also given is the global and hemispheric average northward transports. In January the new physics is producing a net convergence in the northern hemisphere from approximately 10°N to 30°N, while in model II the convergence was occurring farther poleward, from approximately 20°N to 50°N; overall, model II had about 50% greater northward transport in the northern hemisphere. During July, southward transports are now greater with model II′ physics from 20°N to 20°S, including cross-equatorial transport, resulting in greater southern hemisphere concentrations on the yearly average (Figure 6). Southward transports in the southern hemisphere have increased by about 35% with the newer physics.

The differences in total transports at relevant latitudes are given in Figure 7 (bottom), along with the vertically integrated northward values. During January at 32°N the transports are

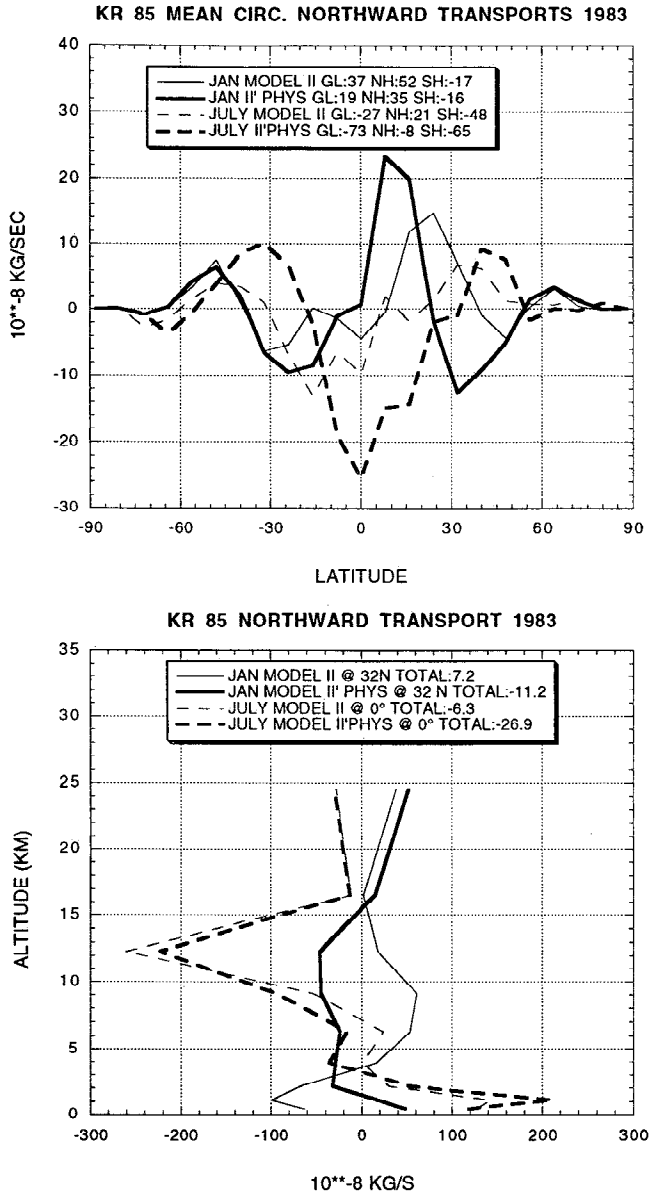

Figure 7. Krypton 85 vertically integrated mean circulation northward transports (top) and vertical profile of total northward transports at 32°N for January and 0° for July (bottom). Global, hemispheric, and total values are indicated in the respective figures. Results are shown for model II and model II′ physics for 1983.

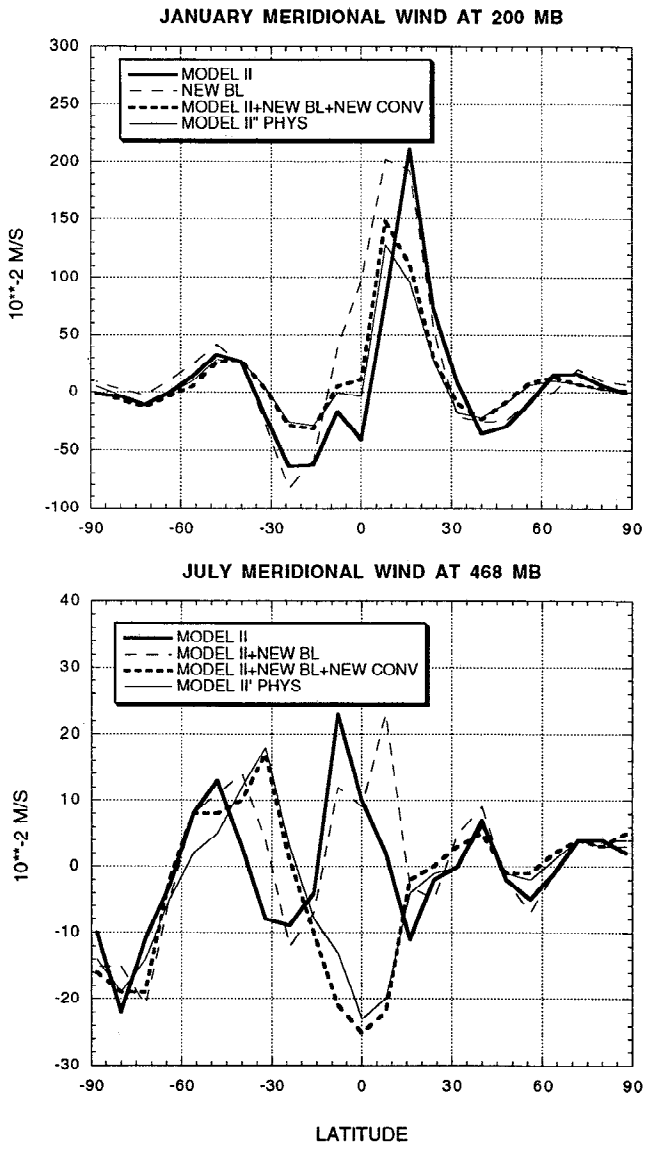

Figure 8. Mean meridional wind at 200 mbar for January (top) and 468 mbar for July (bottom). Results are shown for various model development runs.

southward throughout much of the troposphere with model II′ physics, while they are northward in model II. This is the result of a change in the direction of the mean meridional wind at this latitude (Figure 8, top); note that at 200 mbar the model II winds are displaced northward of those of the newer runs from about 15°S to 40°N. During July there is some 4 times greater southward transport across the equator with the newer physics, the result of more southward flow in the midtroposphere, again a function of the zonal average meridional wind differences (Figure 8, bottom). The net result for the annual average total transport is that southward transports have increased from the equator to 20°S with model II′ physics for both CFC-11 and ^{85}Kr (Figure 9).

The mean circulation changes are associated with changes in precipitation. Figure 10 gives the zonally averaged precipitation for January and July, compared with observations. In January, model II precipitation peaked north of the equator, whereas with the new physics, the peak is at the proper latitude. In July all model simulations shown have too much precipitation between the equator and 10°S, although model II shows the greatest discrepancy.

The precipitation anomalies are associated with misplaced mean circulations. In January the circulation and transports were shifted too far north of the equator (Figures 8, 9), so that by July, species concentrations were not close enough to the equator to be swept into the southern hemisphere (Figure 7). Comparison with observations [*Oort*, 1983; *Trenberth*, 1992] indicates that the meridional wind peak in January should be between 0° and 10°N, as occurs with the newer physics. Furthermore, the equatorial midtropospheric wind circulation in July was of the wrong sign to produce interhemispheric trans-

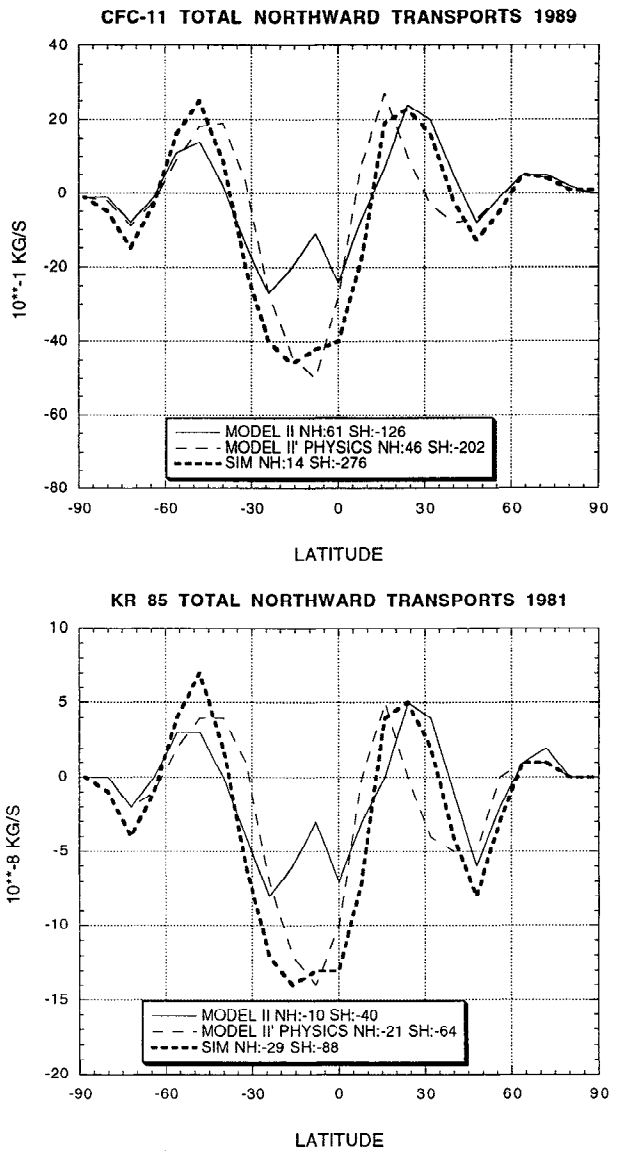

Figure 9. Total model northward transport of CFC-11 (top) in 1989 and ^{85}Kr (bottom) in 1981. Northern and southern hemisphere values are indicated.

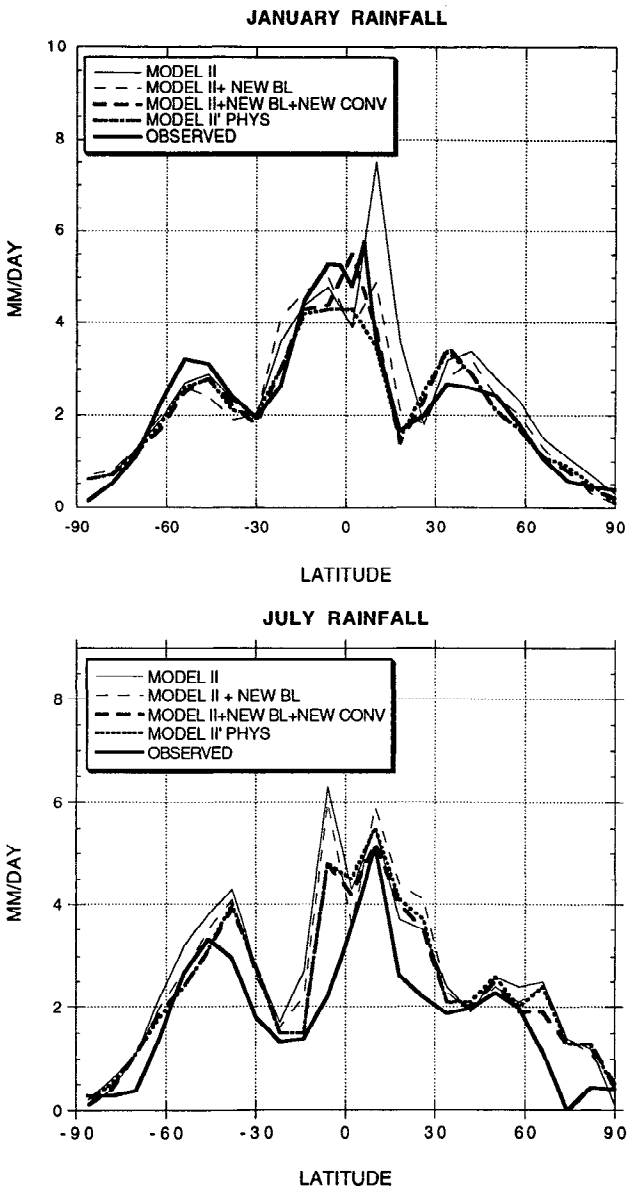

Figure 10. Zonally averaged precipitation during January (top) and July (bottom). Observations are from *Schutz and Gates* [1971, 1972].

port. Observations [*Oort*, 1983; *Trenberth*, 1992] are somewhat inconclusive as to which circulation is more appropriate, because this is apparently a region which experiences significant meridional wind shear and suffers from relatively sparse longitudinal coverage to produce a meaningful "zonal average." The actual increase in interhemispheric transport occurred at the longitudes of the tropical continents in conjunction with the altered precipitation field and meridional circulation.

The processes responsible for the increased interhemi-

Table 4. January Peak Hadley Cell Circulation Intensities and Locations

Experiment	January Peak Intensity, 10^9 kg s^{-1}	January Latitude of Peak	July Peak Intensity, 10^9 kg s^{-1}	July Latitude of Peak
Observed [*Piexoto and Oort*, 1992]	180–200	8°N	180–200	8°S
Model II	137	16°N	146	8°S
Model II′ physics	122	8°N	143	8°S
Model II′ physics + QUS	150	8°N	172	8°S
Model II′ physics + QUS + mom mix	144	8°N	191	8°S
SIM	165	8°N	185	8°S
SIM, 18L	150	8°N	180	8°S

Table 5. Radon 222 Sources and Sinks

	Description
Period of simulation	6 years
Initial conditions	globally uniform concentration of 1.0×10^{-22} kg tracer/kg air
Source	from decay of radium in soils; land, surface air temperature > 273 K: 3.2×10^{-16} kg/m^2/d; land, surface air temperature <273 K: 1.0×10^{-16} kg/m^2/d; ocean, 1.6×10^{-18} kg/m^2/d; ice, zero emission
Sink	radioactive decay, with a first-order loss rate constant; $k = 2.1 \times 10^{-6}$ s^{-1} (corresponding to a lifetime of 5.5 days, or a half-life of 3.8 days)

spheric transport with model II′ physics are the changes in the boundary layer and convection parameterizations. Their impact can be diagnosed from the meridional wind changes shown in Figure 8 as well as the associated precipitation changes (Figure 10). In January the new boundary layer reduced the excessively large precipitation maximum north of the equator (Figure 10, top), shifting the meridional wind maximum closer to the equator (Figure 8, top). Adding the

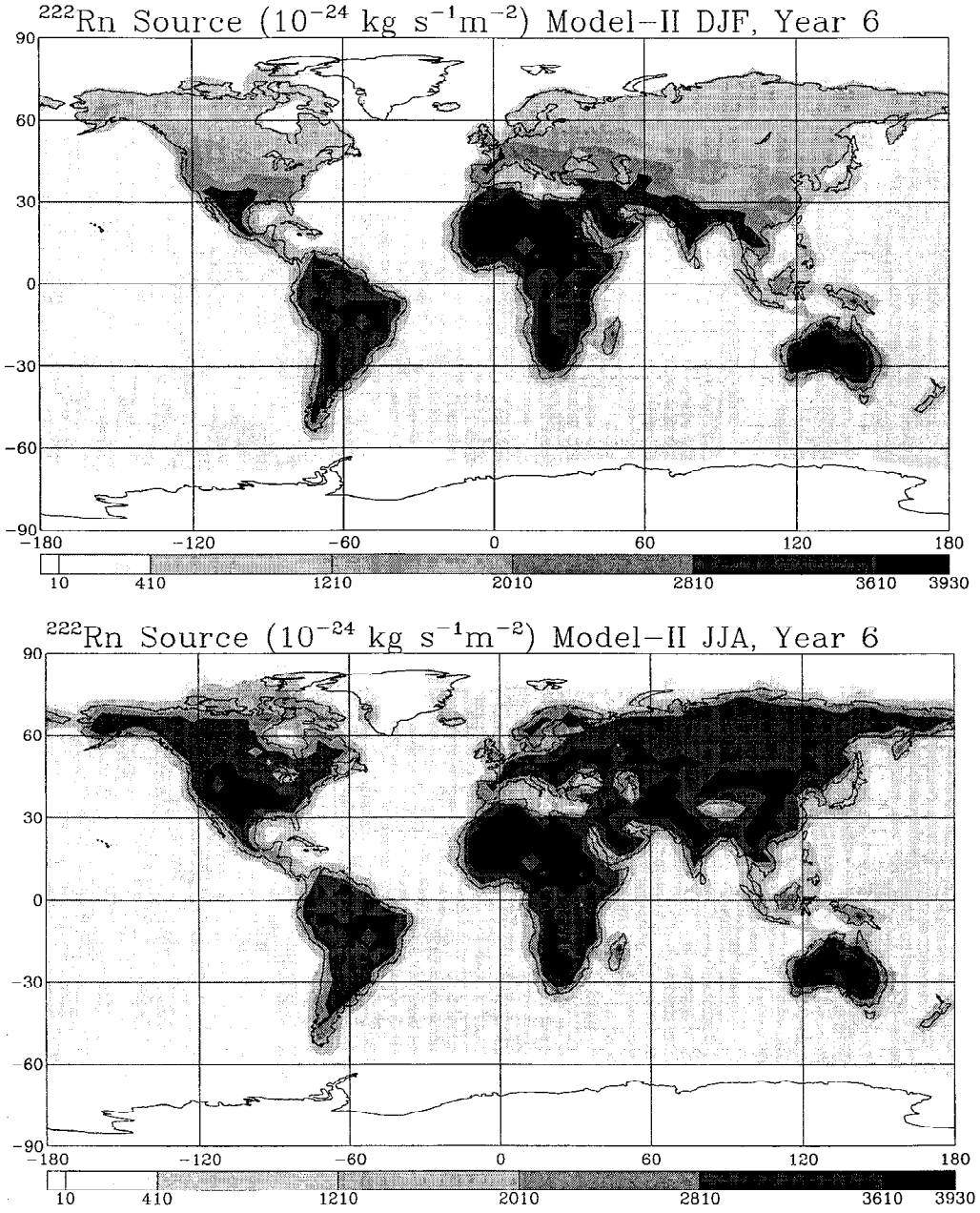

Figure 11a. Geographical distribution of the source of ^{222}Rn for December through February (top) and June through August (bottom) for year 6 in model II.

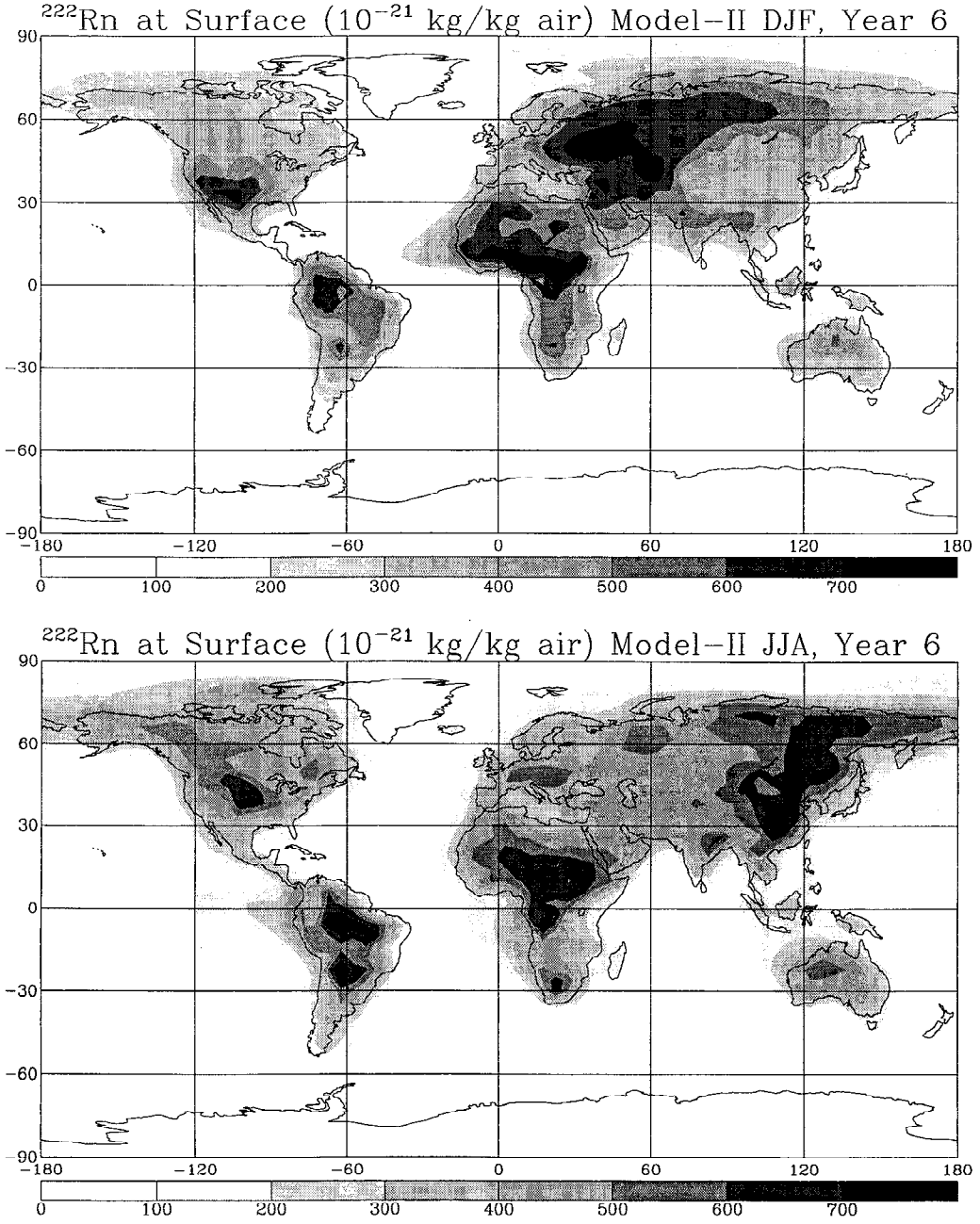

Figure 11b. As in Figure 10 except for ^{222}Rn surface layer concentration.

new convection shifted the peak rainfall even closer to the equator, further reducing the meridional wind from 10° to 30°N.

In July the new boundary layer had minimal influence on the excessive precipitation south of the equator (Figure 10, bottom), or on the meridional wind in the midtroposphere (Figure 8, bottom). Adding the new convection decreased precipitation in this region, although not to observed values; it is indicative of the complex interplay between the boundary layer and the convective parameterizations that when the new convection alone was used, the precipitation was actually higher than in model II. If the model interhemispheric transports are still somewhat too large (Table 3), it may be because of this remaining discrepancy. It should be noted that this feature is apparent in some other models as well [*Boer et al.*, 1991].

As shown in Table 3, other processes had relatively little effect on the interhemispheric transport, even though, with additional model development, the resulting model had a substantially stronger (and more accurate) Hadley circulation in both January and July (Table 4). In fact, adding momentum mixing, which intensifies the Hadley circulation during some seasons, actually reduced the interhemispheric mixing time. Apparently, it is the latitude of the circulation center, rather than its magnitude, which is of prime importance in the model for determining interhemispheric transport. This result is also of potential relevance for the effect of climate change on interhemispheric transport.

The interhemispheric transport time may also be associated with the numerical scheme used for transport of the tracers. For example, including sub-grid-scale diffusion in the CTM reduced the transport time by a factor of 2 [*Prather et al.*, 1987].

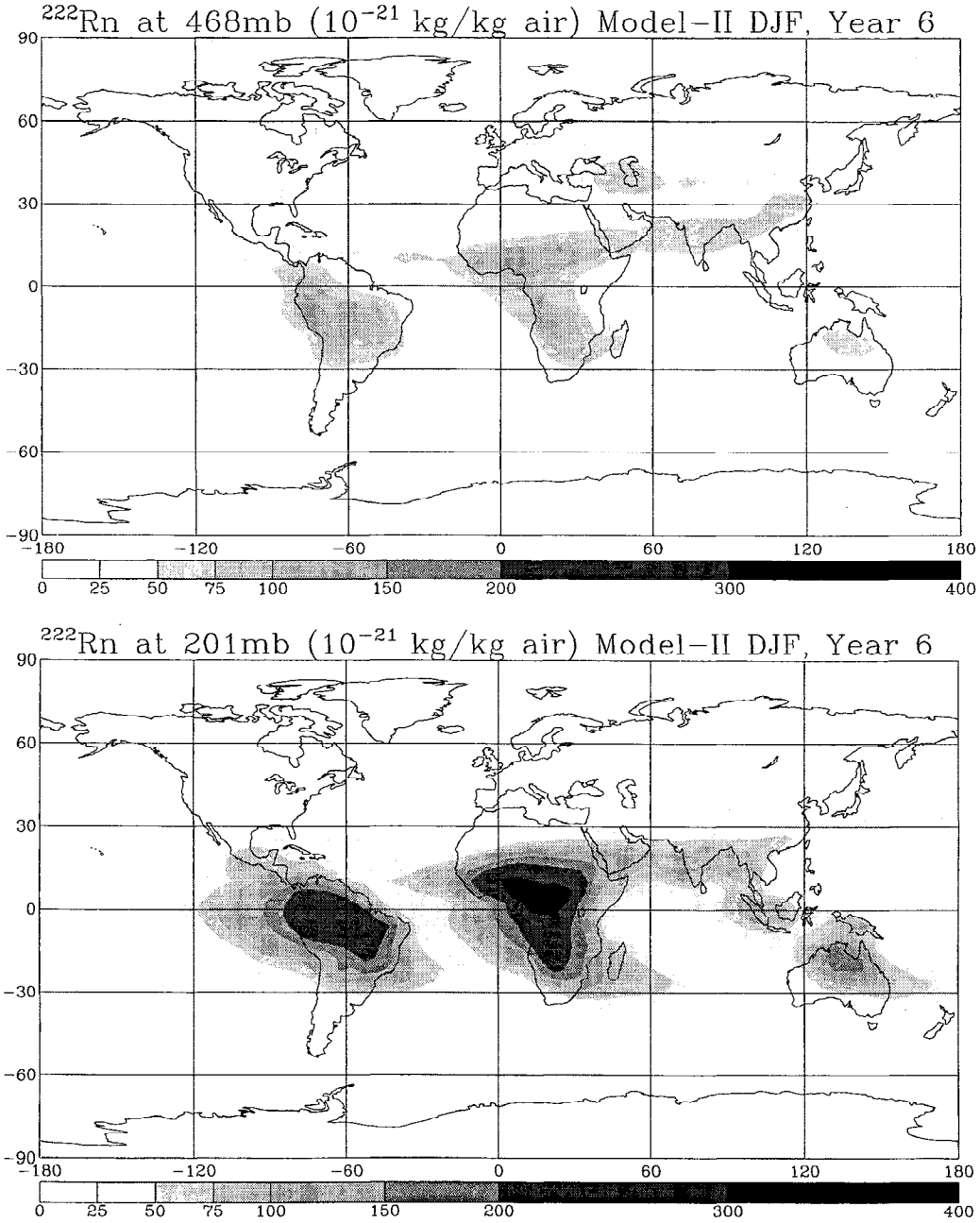

Figure 12. Geographical distribution of ^{222}Rn in layer 5 (468 mbar) (top) and layer 7 (200 mbar) (bottom) for year 6 in model II in December through February and June through August.

The model results discussed above used the linear upstream scheme [*Russell and Lerner*, 1981] which is somewhat more diffusive than a quadratic upstream scheme, or its mathematical equivalent, second-order moments [*Prather*, 1986]. An additional test was run with SIM using the quadratic upstream scheme for tracer advection; as shown in Table 3, transport times were only slightly larger. However, stratospheric concentrations were somewhat reduced, indicative of the ability of this scheme to maintain strong gradients. The impact of tracer advection schemes on tropospheric-stratospheric exchange will be discussed in detail in part 2 of this series.

4.2. Vertical Transport

Radon 222 is used to assess the vertical transport in the model. The characteristics of the simulation initial conditions, sources, and sinks are shown in Table 5. The primary emission of ^{222}Rn is due to radium decay in soils, with larger values occurring at temperatures above the freezing point. There is also a small ocean source [*Jacob and Prather*, 1990; *Balkanski and Jacob*, 1990; *Balkanski et al.*, 1992]. Radioactive decay is the sink, with an exponential lifetime of 5.5 days (a half-life of 3.8 days). Therefore ^{222}Rn is a better test of fast transport processes, like convection, than of the large-scale circulation.

The geographical distribution of the source in year 6 for the two solstice seasons is shown in Figure 11a, while the surface layer values from model II are shown in Figure 11b. In the northern hemisphere the land source is larger in summer, due to warmer soil temperatures, but because of the increased convective mixing, low-level values are somewhat smaller over Eurasia.

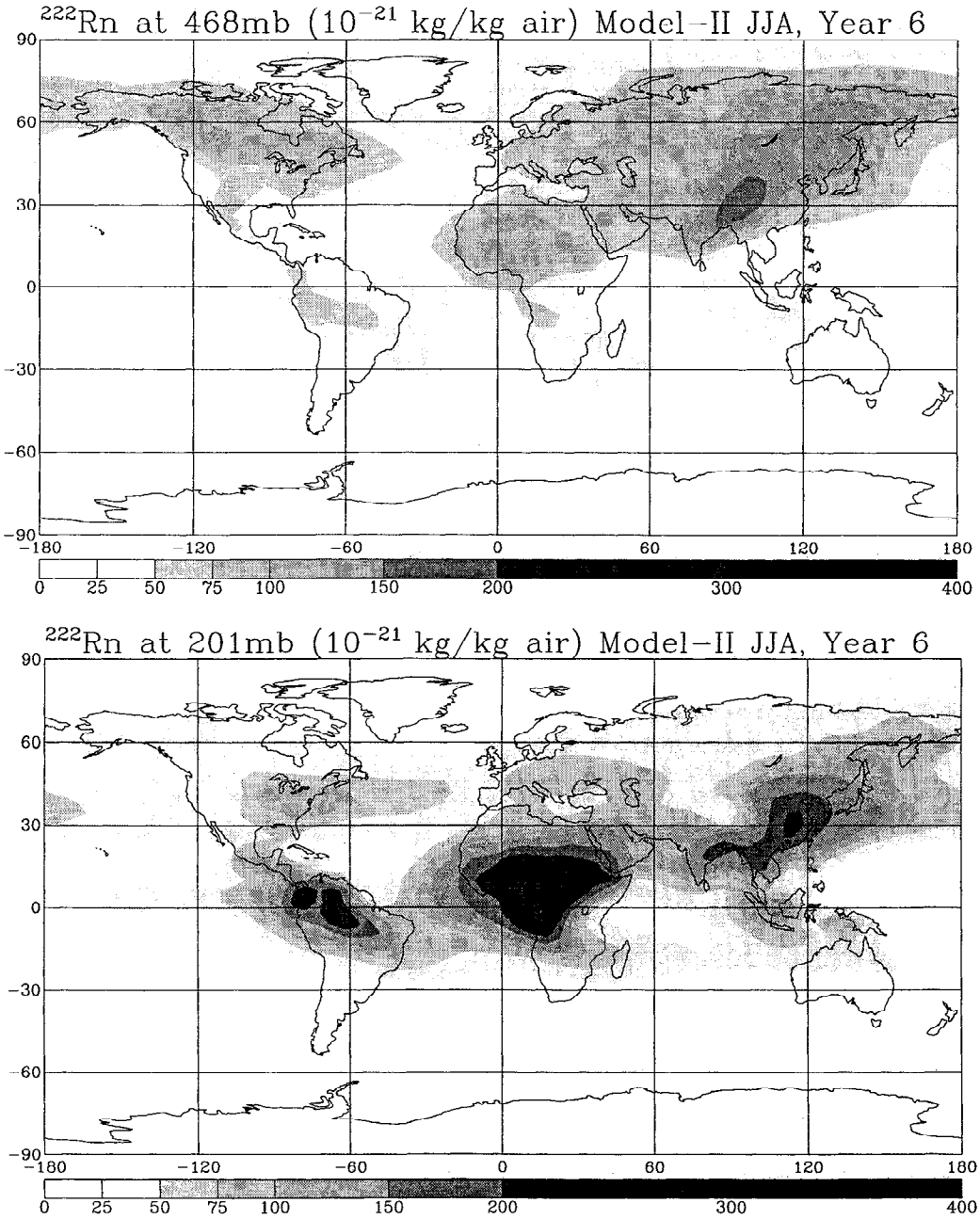

Figure 12. (continued)

The geographical distribution in the middle troposphere (468 mbar, approximately 6 km) and upper troposphere (200 mbar, approximately 12 km) is shown for the two solstice seasons in Figure 12 (top, bottom) for model II. Only the most extreme tropical convection raises significant amounts of radon to the upper troposphere, where values are often larger than in the middle troposphere.

The global annual average vertical profile of ^{222}Rn is given in Figure 13 for different model runs. With the new physics, values have decreased above 7 km. None of the other model changes appear to make any real difference, including the use of QUS for tracer advection, although increased vertical resolution does result in slightly larger values above 10 km.

Zonal annual average distributions as a function of pressure altitude are shown in Figure 14a for model II (top) and model II′ physics (bottom), and Figure 14b for SIM with nine vertical layers (top) and with 18 layers (bottom). The primary difference can be seen to occur in the tropics, where most of the high-altitude distribution is located. Figure 15 shows the latitudinal average values at 200 mbar, where it is obvious that there is little difference poleward of 30° latitude.

The various vertical transport processes are given in Figure 16 for the global, annual average. Convective transports (top) increase the vertical concentration in model II relative to the other runs from 6 to 16 km. The large-scale vertical transports (bottom) in that run were then responsible for lifting this excess to higher levels. The effect is primarily due to the mean circulation; the eddy transports by themselves, as shown in Figure 16 (middle), are only slightly higher above 16 km.

Up to 15 km the moist convective exchange of air mass is larger in model II (Figure 17). The new moist convection scheme lifts a smaller amount of mass at each time step, em-

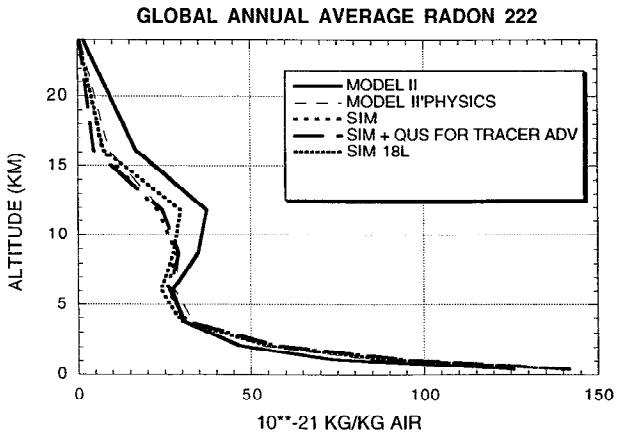

Figure 13. Global annual average vertical profile of ^{222}Rn.

ploys entrainment for low-level convection, and incorporates explicit downdrafts, all of which have the effect of limiting vertical mass exchange. The 18 layer model gives somewhat higher mass fluxes, presumably because the finer vertical resolution allows for more convection when stability is not averaged over broad levels. It then also has somewhat greater values of ^{222}Rn in the upper troposphere (Figures 13–15).

Given the distinct difference in results, it should be straightforward to determine which convective approach is more accurate. Unfortunately, most of the observations have been made at a very few midlatitude locations [e.g., *Liu et al.*, 1984], and as is apparent in Figures 14 and 15, the differences are small outside of the tropics.

Only a few observations are available from the tropics. *Kritz et al.* [1993] found values near Darwin, Australia, in summer of around 30×10^{-21} kg/kg air at 15 km dropping to around 20×10^{-21} kg/kg air at 16 km, although several observations of around 100×10^{-21} kg/kg air occurred in the cirrus shield of a tropical cyclone. They concluded that tropospheric values of 85×10^{-21} kg/kg air, consistent with the observed inventory of stratospheric ^{210}Pb, were probably more representative of the air which goes into the stratosphere (i.e., convective plumes, not often observed because of adverse weather conditions); lower values could also have been present due to mixing with depleted stratospheric air. In comparison, the model II physics had time-averaged values for this season of 64×10^{-21} kg/kg air at 16 km over Darwin, while the model II′ physics had values of 12×10^{-21}. Given the uncertainty in the observed time-averaged values, it is not clear which is a more accurate assessment. Moist convection occurs some 30% of the time in the model in this region during summer; if that is true for the real world as well, and if the convective value is 85×10^{-21} kg/kg air, while the nonconvective value is 20×10^{-21} kg/kg air, then the real world time-averaged value would be around 40×10^{-21} kg/kg air, in between the value from the two convective schemes, and closer to the 18 layer result. Obviously, more tropical observations are needed. It should be noted that the reduced values shown with model II′ physics are more consistent with CTM results produced by other models [*IPCC*, 1994].

5. Discussion and Conclusions

Several other results of interest for tropospheric chemistry purposes can be derived from these experiments. Venting of the boundary layer is of primary importance in air pollution studies. While the CFC-11 distribution used for these tests was not particularly well formulated for investigating pollution results [*Williamson et al.*, 1992], the difference in low-level concentrations can be assessed. At the grid box of Adrigole, Ireland, peak hourly values in model II amounted to 15 ppt, with average variances of 17 ppt^2. With model II′ physics the peak

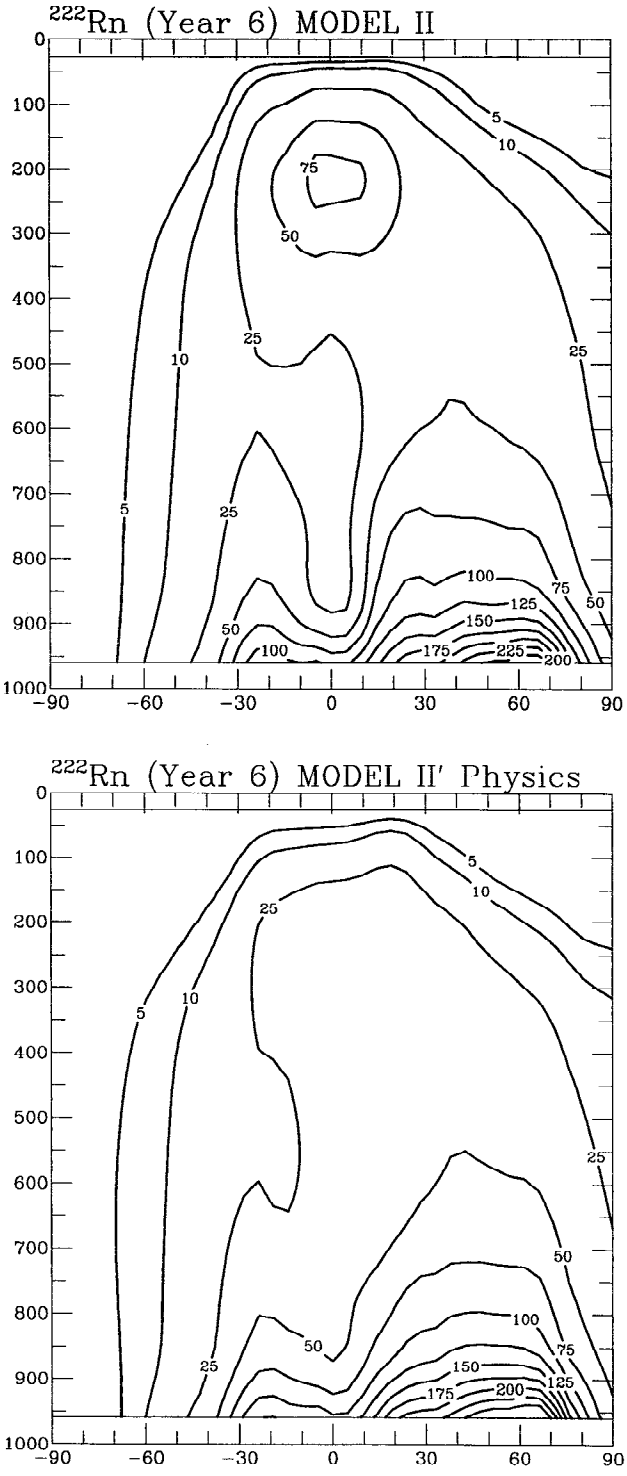

Figure 14a. Zonal annual average latitude-height distributions of ^{222}Rn for model II (top) and model II′ physics (bottom) in year 6. Units are 10^{-21} kg/kg air.

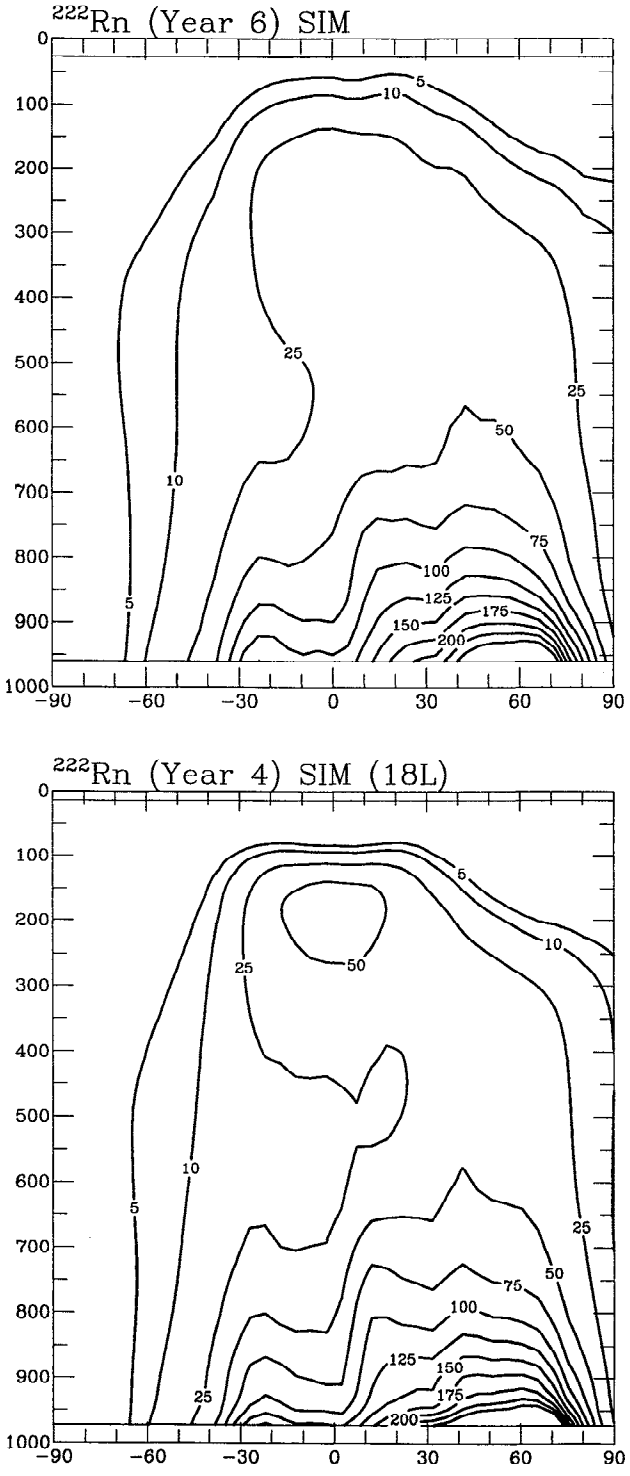

Figure 14b. As in Figure 14a except for Summer Institute Model (SIM) with 9 layers (top) and SIM with 18 layers (bottom).

values exceeded 20 ppt, with average variances of 35 ppt^2, associated with the reduced convective mass fluxes in the new convection scheme. Addition of improved numerics in SIM, which had the effect of moving air masses more rapidly, actually lowered the magnitude of peak pollution events (variances of 25 ppt^2), while the 18-layer version of SIM, with increased resolution in the boundary layer and hence larger near-surface concentrations, produced peak values of greater than 30 ppt

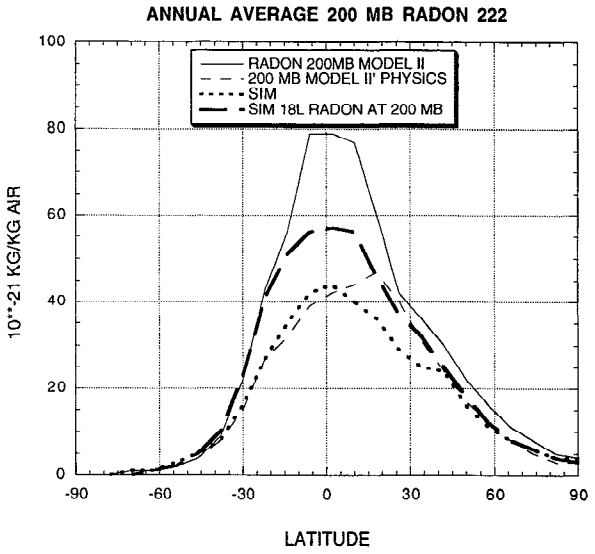

Figure 15. Latitudinal average 200 mbar values of ^{222}Rn.

and average variances back up to 35 ppt^2. Higher values are more realistic, although to provide values as large as observed (e.g., variances of 125 ppt^2 [*Cunnold et al.*, 1986]) requires much finer horizontal resolution as well [*Prather et al.*, 1987].

Observed CFC autocorrelations at Adrigole had half-height half-width durations of 2 days and an extended shoulder with elevated concentrations out to 8 days [*Cunnold et al.*, 1986; *Prather et al.*, 1987]. Model II's characteristic timescales were 2 and 10 days, respectively. With new model physics and numerics the timescales dropped to 1.5 and 9 days, indicative of the more rapid movement of air due primarily to the fourth-order momentum scheme. Again, the results are of use primarily for intermodel comparison, given the limitations of this study for pollution events; *Hartley et al.*, [1994], using more detailed source functions, have shown how CFC-11 can be used to diagnose the accuracy of the CCM-2 storm tracks around Ireland.

The incorporation of on-line tracers in the course of model development is useful in analyzing higher-order transport fields for passive tracers, thereby providing for ongoing assessment of the utility of these models for tropospheric chemistry studies. In addition, they provide complimentary evidence for changes which appear in more climate-related diagnostics, such as precipitation. Given the emerging emphasis on societal needs, model development will probably continue to focus primarily on the parameters necessary for climate simulations. However, without an ongoing assessment of the less obvious flux characteristics, it will be difficult to optimize GCMs for tropospheric chemistry purposes. The passive tracers provide information on model properties which is often easier to deduce than from other, more interactive diagnostics. We encourage the use of such tracers in GCM model development.

The primary results of this work are as follows:

1. CFC-11 and ^{85}Kr provide duplicate information about interhemispheric transports. In these experiments, changes in the boundary layer parameterization and convection altered the precipitation and meridional wind fields associated with the general circulation, allowing for more accurate interhemispheric transports. Other processes, while increasing the magnitude of the tropical mean circulation cells, did not produce

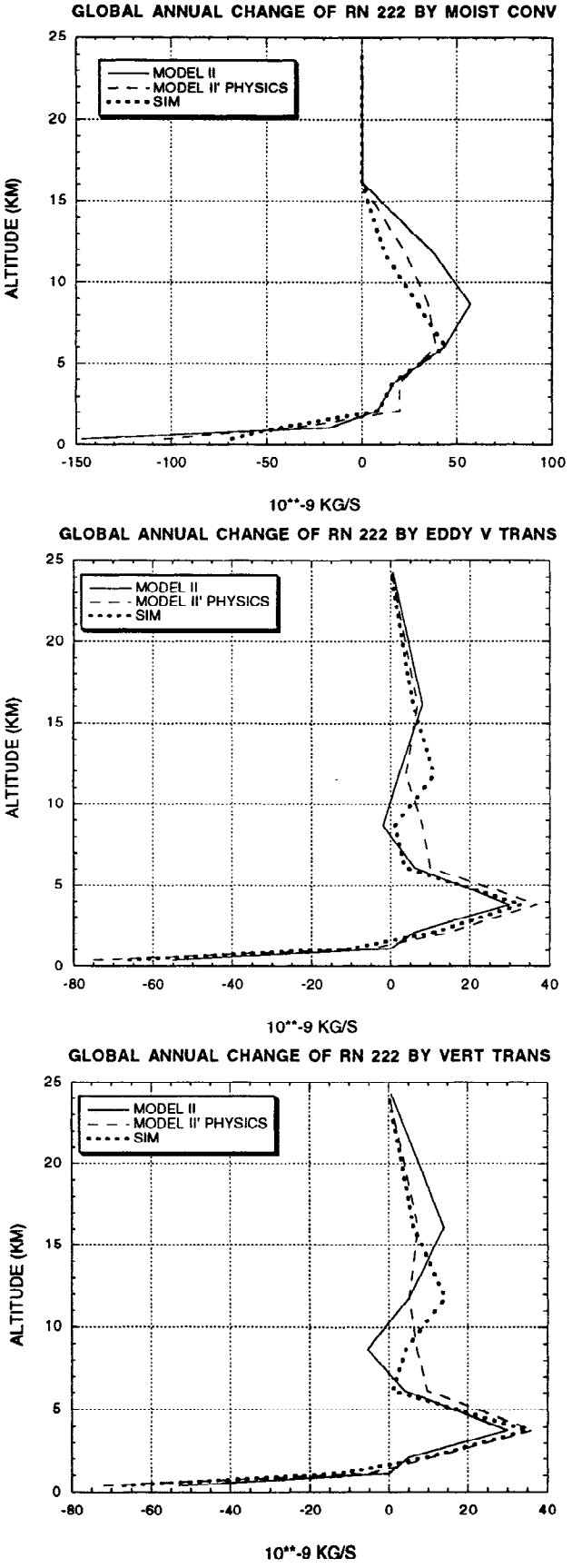

Figure 16. Global, annual average change of ^{222}Rn by various processes: moist convection (top), eddy vertical transport (middle), eddy plus mean circulation vertical transport (bottom).

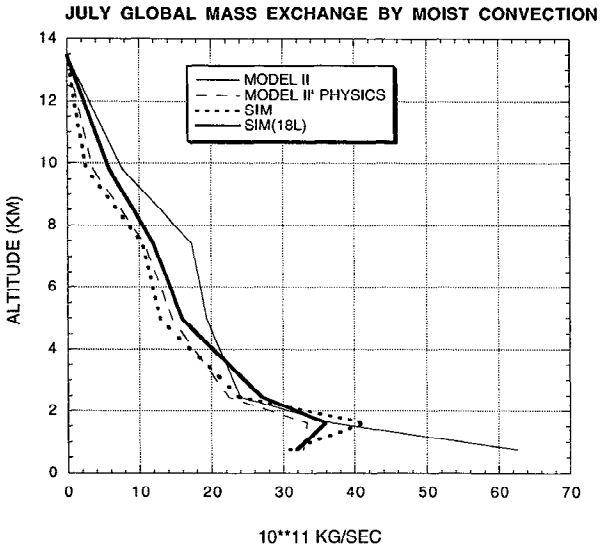

Figure 17. July global average mass exchange by moist convection.

much effect on interhemispheric transport times, presumably because the location of the Hadley cell was unaffected.

2. Radon 222 is useful for evaluating vertical transports in the model associated with convection. The experiments showed that large differences occurred between the old and the new convection schemes in the upper troposphere at locations equatorward of 30° latitude. Unfortunately, the general lack of tropical radon observations prevents us from concluding which scheme is more accurate. It is to be hoped that this situation can be remedied with additional observations in the foreseeable future.

While the additional model changes did not have much effect on these transports, for tropospheric chemistry as well as climate simulation purposes, other modeled parameters are important, such as temperature, water vapor, and cloud cover distributions. These quantities are affected by the different physical/numerical parameterizations. A final evaluation of model "improvement" obviously needs to account for their simulation as well.

In this paper we have focused on horizontal and vertical transports within the troposphere. In subsequent papers we will explore the effect of model resolution and parameterizations on tropospheric/stratospheric exchange and on transport within the stratosphere.

Acknowledgments. We thank D. Jacob, M. Prather, and C. Spivakovsky for extensive guidance in setting up the tracer sources and sinks and continued encouragement during the course of these experiments. The tracer component of this work was supported by the NASA Atmospheric Chemistry Modeling and Analysis program, while climate model development is supported by the NASA Climate Modeling program.

References

Abramopoulos, F., C. Rosenzweig, and B. Choudhury, Improved ground hydrology calculations for global climate models (GCMs): Soil water movement and evapotranspiration. *J. Clim.*, *1*, 921–941, 1988.

Arakawa, A., Design of the UCLA GCM, *Tech. Rep. 7*, Dep. of Meteorol., Univ. of Calif., Los Angeles, 116 pp., 1972.

Balkanski, Y. J., and D. J. Jacob, Transport of continental air to the subantarctic Indian Ocean, *Tellus*, *42*, 62–75, 1990.

Balkanski, Y. J., D. J. Jacob, R. Arimoto, and M. A. Kritz, Distribution of ^{222}Rn over the North Pacific: Implications for continental influences, *J. Atmos. Chem.*, *14*, 353–374, 1992.

Boer, G. J., et al., *An Intercomparison of the Climates Simulated by 14 Atmospheric General Circulation Models*, World Clim. Res. Program, *WCRP-58, WMO/TD-425*, 37 pp., 1991.

Boyle, J. S., Sensitivity of dynamical quantities to horizontal resolution in a climate simulation with the ECMWF atmospheric general circulation model (cycle 33), *PCMDI Rep. 6*, 37 pp., Lawrence Livermore Nat. Lab., Livermore, Calif, 1992.

Charles, C. D., D. Rind, J. Jouzel, R. Koster, and R. G. Fairbanks, Glacial-interglacial changes in moisture sources for Greenland: Influences on the ice core record, *Science*, *263*, 508–510, 1994.

Chin, M., D. J. Jacob, J. W. Munger, D. D. Parrish, and B. G. Doddridge, 1994: Relationship of ozone and carbon monoxide over North America, *J. Geophys. Res.*, *99*, 14,565–14,573, 1994.

Cole, J., D. Rind, and R. Fairbanks, Isotopic responses to interannual climate variability simulated by the GISS GCM, *Quat. Sci. Rev.*, *12*, 387–406, 1993.

Cunnold, D. M., R. G. Prinn, R. A. Rasmussen, P. G. Simmonds, F. N. Alyea, C. A. Cardelino, A. J. Crawford, P. J. Fraser, and R. D. Rosen, The atmospheric lifetime experiment 3, Lifetime methodology and application to three years of $CFCl_3$ data, *J. Geophys. Res.*, *88*, 8379–8400, 1983.

Cunnold, D. M., R. G. Prinn, R. A. Rasmussen, P. G. Simmonds, F. N. Alyea, C. A. Cardelino, A. J. Crawford, P. J. Fraser, and R. D. Rosen, Atmospheric lifetime and annual release estimates for $CFCl_3$ and CF_2Cl_2 from 5 years of ALE data, *J. Geophys. Res.*, *91*, 10,797–10,817, 1986.

Cunnold, D. M., P. J. Fraser, R. F. Weiss, R. G. Prinn, P. G. Simmonds, F. N. Alyea, and A. J. Crawford, Global trends and annual releases of $CFCl_3$ and CF_2Cl_2 estimated from ALE/GAGE and other measurements from July 1978 to June 1991, *J. Geophys. Res.*, *99*, 1107–1126, 1994.

DelGenio, A. D., and M-S Yao, Efficient cumulus parameterization for long-term climate studies: The GISS scheme, in *Cumulus Parameterization*, AMS Monogr. Ser., edited by K. Emanuel and D. Raymond, Am. Meteorol. Soc., Boston, Mass., 1992.

Del Genio, A. D., and M.-S. Yao, A prognostic cloud water parameterization for global climate models, *J. Clim.*, in press, 1995.

Fung, I., K. Prentice, E. Matthews, J. Lerner, and G. Russell, Three-dimensional tracer model study of atmospheric CO_2: Response to seasonal exchanges with the terrestrial biosphere, *J. Geophys. Res.*, *88*, 1281–1294, 1983.

Fung, I., J. John, J. Lerner, E. Matthews, M. Prather, L. P. Steele, and P. J. Fraser, Three-dimensional model synthesis of the global methane cycle, *J. Geophys. Res.*, *96*, 13,033–13,066, 1991.

Hall, T., and M. J. Prather, Simulations of the trend and annual cycle in stratospheric CO_2, *J. Geophys. Res.*, *98*, 10,573–10,581, 1993.

Hansen, J., G. Russell, D. Rind, P. Stone, A. Lacis, S. Lebedeff, R. Ruedy, and L. Travis, Efficient three-dimensional global models for climate studies: Models I and II, *Mon. Weather Rev.*, *111*, 609–662, 1983.

Hartley, D., D. Williamson, P. Rasch, and R. Prinn, An examination of tracer transport in the NCAR CCM2 by comparison of $CFCl_3$ simulations with ALE/GAGE observations, *J. Geophys. Res.*, *99*, 12,885–12,896, 1994.

International Panel on Climate Control (IPCC), *Climate Change, The IPCC Scientific Assessment*, 339 pp., Cambridge Univ. Press, New York, 1990.

IPCC, *Climate Change 1992*, 200 pp., Cambridge Univ. Press, New York, 1992.

IPCC, *Climate Change 1994*, 200 pp., Cambridge Univ. Press, New York, 1994.

Jacob, D. J., and M. J. Prather, Radon-222 as a test of convective transport in a general circulation model, *Tellus*, *42*, 118–134, 1990.

Jacob, D. J., M. J. Prather, S. C. Wofsy, and M. B. McElroy, Atmospheric distribution of ^{85}Kr simulated with a general circulation model, *J. Geophys. Res.*, *92*, 6614–6626, 1987.

Jacob, D. J., S. Sillman, J. A. Logan, and S. C. Wofsy, Least independent variables method for simulation of tropospheric ozone, *J. Geophys. Res.*, *94*, 8497–8510, 1989.

Jouzel, J., G. L. Russell, R. J. Suozzo, R. D. Koster, M. W. C. White, and W. S. Broecker, Simulations of the HDO and $H_2{}^{18}O$ atmospheric cycles using the NASA GISS general circulation model: The seasonal cycle for present-day conditions, *J. Geophys. Res.*, *92*, 14,739–14,760, 1987.

Jouzel, J., R. D. Koster, R. J. Suozzo, G. L. Russell, J. W. C. White, and W. S. Broecker, Simulations of the HDO and $H_2{}^{18}O$ atmospheric cycles using the NASA GISS general circulation model: Sensitivity experiments for present-day conditions, *J. Geophys. Res.*, *96*, 7495–7508, 1991.

Kalnay-Rivas, E., A. Bayliss, and J. Storch, The 4th order GISS model of the global atmosphere, *Cont. Atmos. Phys.*, *50*, 306–311, 1977.

Kaye, J. A., S. A. Penkett, and F. M. Ormond (Eds.), *Report on Concentrations, Lifetimes and Trends of CFCs, Halons, and Related Species*, *NASA Ref. Publ. 1339*, 169 pp., 1994.

Kritz, M. A., S. Rosner, K. K. Kelly, M. Loewenstein, and K. R. Chan, Radon measurements in the lower tropical stratosphere: Evidence for rapid vertical transport and dehydration of tropospheric air, *J. Geophys. Res.*, *98*, 8725–8736, 1993.

Liu, S. C., J. R. McAfee, and R. J. Cicerone, Radon 222 and tropospheric vertical transport, *J. Geophys. Res.*, *89*, 7291–7297, 1984.

Oort, A., *Global Atmospheric Circulation Statistics*, *NOAA Prof. Pap. 14*, 180 pp., U.S. Dep. of Comm., Washington, D. C., 1983.

Piexoto, J. P., and A. H. Oort, *Physics of Climate*, 520 pp., Am. Inst. of Phys., New York, 1992.

Pinto, J. P., Y. L. Yung, D. Rind, G. L. Russell, J. A. Lerner, J. E. Hansen, and S. Hameed, A general circulation model study of atmospheric carbon monoxide, *J. Geophys. Res.*, *88*, 3691–3702, 1983.

Prather, M., Numerical advection by conservation of second-order moments, *J. Geophys. Res.*, *91*, 6671–6681, 1986.

Prather, M., Report for WCRP Workshop on Long-Range Transport of Trace Gases 10–14 December 1990, Special Numerical Experiment: Simulation of $CFCl_3$ as a test for 3-D atmospheric models, World Meteorol. Organ., Geneva, 1992.

Prather, M., and E. E. Remsberg (Eds.), *The Atmospheric Effects of Stratospheric Aircraft: Report of the 1992 Models and Measurements Workshop*, vol. 2, in *Comparisons With Global Atmospheric Measurements*, *NASA Ref. Publ. 1292*, 1993.

Prather, M., M. McElroy, S. Wofsy, G. Russell, and D. Rind, Chemistry of the global troposphere: Fluorocarbons as tracers of air motion, *J. Geophys. Res.*, *92*, 6579–6614, 1987.

Prather, M., M. Garcia, R. Suozzo, and D. Rind, Global impact of the Antarctic ozone hole: Dynamical dilution with a 3-D chemical transport model, *J. Geophys. Res.*, *95*, 3449–3472, 1990.

Prinn, R. G., et al., The Atmospheric Lifetime Experiment, 1, Instrumentation and overview, *J. Geophys. Res.*, *88*, 8353–8367, 1983.

Rind, D., R. Suozzo, N. K. Balachandran, A. Lacis, and G. L. Russell, The GISS global climate/middle atmosphere model, I, Model structure and climatology, *J. Atmos. Sci.*, *45*, 329–370, 1988.

Rosenzweig, C., and F. Abramopoulos, Land-surface model development for the GISS GCM, *J. Clim.*, in press, 1995.

Russell, G., and J. Lerner, A new finite differencing scheme for the tracer transport equation, *J. Appl. Meteorol.*, *20*, 1483–1498, 1981.

Schutz, C., and W. Gates, 1971, 1972: Global climatic data for surface, 800 mb, 400 mb, *Rep. R-915-ARPA*, *Rep. R-1029-ARPA*, Rand Corp., Santa Monica, Calif., 1971, 1972.

Trenberth, K. E., *Global Analyses From ECMWF*, *NCAR Tech. Note TN-373+STR*, Natl. Cent. for Atmos. Res., Boulder, Colo., 1992.

Williamson, D., P. Rasch, and D. Hartley, WCRP CFC-11 simulations by the NCAR CCM2, Report for WCRP Workshop on Long-Range Transport of Trace Gases 10-14 December 1990, Special Numerical Experiment: Simulation of $CFCl_3$ as a test for 3-D atmospheric models, edited by M. Prather, World Meteorol. Organ., Geneva, 1992.

World Climate Research Program (WCRP), An intercomparison of the climates simulated by 14 atmospheric general circulation models, edited by G. J. Boer, et al., *WCRP-58*, *WMO/TD-425*, World Meteorol. Organ., Geneva, 1991.

World Meteorological Organization (WMO), *Scientific Assessment of Ozone Depletion: 1991*, WMO/UNEP, WMO Global Ozone Res. and Monit. Proj. *WMO Rep. 25*, Geneva, 1992.

J. Lerner, Science Systems and Applications, Inc., New York, N.Y. 10025.

D. Rind, NASA Goddard Space Flight Center, Institute for Space Studies, 2880 Broadway, New York, NY 10025.

(Received November 30, 1994; revised October 17, 1995; accepted January 31, 1996.)